Geophysical Journal International

Geophys. J. Int. (2011) doi: 10.1111/j.1365-246X.2011.5173.x

EXPRESS LETTER

Wavefront healing renders deep plumes seismically invisible

Yong Keun Hwang,[1] Jeroen Ritsema,[1] Peter E. van Keken,[1] Saskia Goes[2] and Elinor Styles[2]

[1]*Department of Geological Sciences, University of Michigan, Ann Arbor, MI 48109, USA. E-mail: ykhwang@umich.edu*
[2]*Department of Earth Science and Engineering, Imperial College London, London, SW7 2AZ, UK*

Accepted 2011 July 28. Received 2011 July 19; in original form 2011 April 15

SUMMARY

Since W. J. Morgan proposed that intraplate volcanism at some Pacific hotspots is caused by hot plumes rising from the lower mantle, geophysicists have been actively pursuing physical evidence for mantle plumes. Several seismic studies have mapped low-velocity anomalies below a number of hotspots. However, the association of low-velocity structures with plume tails has remained controversial given the debate on whether lower-mantle plumes impart observable traveltime or amplitude perturbations on seismic waves. Using high-resolution numerical simulations of plume ascent through the mantle and their effects on waveforms, we demonstrate that the delay of shear waves by plume tails at depths larger than 1000 km are immeasurably small (<0.2 s) at seismic periods commonly used in waveform analysis. Therefore, we conclude that narrow lower mantle plumes are not detectable.

Key words: Seismic tomography; Computational Seismology; Wave scattering and diffraction; Wave propagation.

1 INTRODUCTION

A hotspot is a long-term source of volcanism unexplained by plate boundary processes. Many hotspots are characterized by topographic swells, a relatively fixed mantle-source position leading to volcanic lines with a systematic age progression and distinct radiogenic isotope characteristics. Although mid-plate volcanism in some regions may have a shallow mantle origin (King & Ritsema 2000; Foulger *et al.* 2005), geochemical and geophysical observations link a large number of hotspots to narrow upwellings from the deep mantle (Farley & Neroda 1998; Ito & van Keken 2007). Plumes may have a profound effect on the geologic landscape. They have been implicated in the initiation of continental break-up and massive flood basalt eruptions that trigger climate changes and mass extinctions (Richards *et al.* 1989; Hawkesworth *et al.* 1999).

Numerical and experimental simulations of mantle convection demonstrate that thermal plumes develop from instabilities that naturally arise in thermal boundary layers such as the core–mantle boundary. Plume morphology in a convecting mantle with chemical and phase changes and non-linear rheology may be complex (van Keken 1997; Steinberger & O'Connell 1998; Farnetani & Samuel 2003). However, most simulations show that a plume is characterized by a large 'head' that rises rapidly in the mantle while connected to the boundary layer via a relatively narrow 'tail' (Ribe *et al.* 2007).

Wide-spread acceptance of plumes in Earth's mantle is contingent on an undisputed seismic detection. A number of regional-scale seismic studies suggest the presence of sharp cylindrical velocity anomalies below the lithosphere that cause traveltime delays (Nataf & VanDecar 1993) and wave diffraction (Ji & Nataf 1998). In addition, several hotspots are directly above lower-than-average seismic velocities in the upper mantle (Wolfe *et al.* 1997; Ritsema & Allen 2003) and mid mantle (Montelli *et al.* 2004; Wolfe *et al.* 2009), topographic variations of the 410-km and 660-km discontinuities (Shen *et al.* 1998), and ultra-low-velocity-zones (Helmberger *et al.* 1998) and broad low-shear-velocity regions (Dziewonski *et al.* 2010) at the base of the mantle.

It remains questionable whether these seismic observations can be uniquely linked to plumes. Dynamic plume models that are consistent with the surface observations predict tails that are narrower than 100–200 km in the upper mantle. Under the influence of increasing viscosity and thermal conductivity and decreasing expansivity with depth (van Keken & Gable 1995; Goes *et al.* 2004), plumes may have widths of up to 1000 km in the lower mantle. However, associated wave speed reductions are expected to be less than a percent. Hence, their impact on traversing waves may be minimal.

In this study, we investigate whether dynamically predicted plume structures can be detected seismically by simulating 3-D wave propagation through a set of high-resolution numerical plume models. In particular, we determine whether wavefront healing (Wielandt 1987; Malcolm & Trampert 2011) reduces the traveltime delay due to a low-velocity deep mantle plume to an immeasurably small value at the Earth's surface.

2 PLUME SIMULATIONS

We simulate plumes by solving the coupled Stokes and energy equations for thermally driven convection with modifications for the effects of compressibility and phase changes. The governing

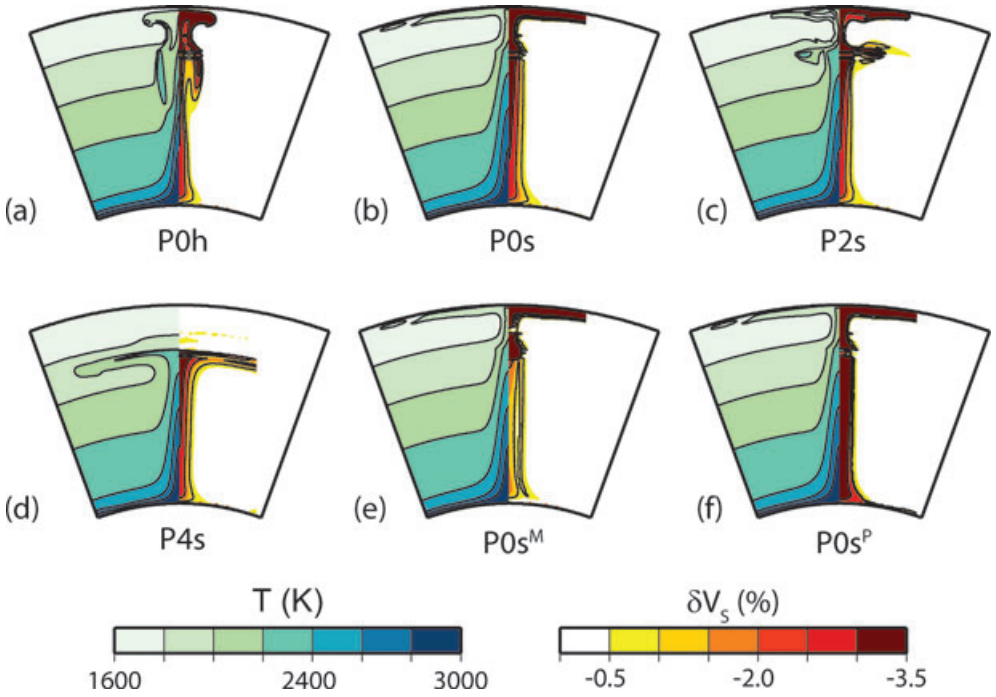

Figure 1. Absolute temperature structures (left half) and shear velocity perturbations (right half) of plume models (a) P0h, (b) P0s, (c) P2s, (d) P4s, (e) $P0s^M$ and (f) $P0s^P$. Temperature (T) structures are in Kelvin (K) and shear velocity anomalies (δV_S) are relative to PREM. The cross-sections are 40° wide and encompass the entire mantle.

equations are based on the conservation of mass, momentum and energy under the anelastic liquid approximation (King *et al.* 2010). These models are similar in design to those described in Leng & Zhong (2010). The numerical simulations employ a high-resolution axisymmetric spherical shell geometry (Lin & van Keken 2006). This geometry preserves the 3-D nature of vertically rising plumes in a spherical Earth and enables us to reproduce Earth-like convective vigour and to simulate plumes with a spatial resolution of a few kilometres near the plume axis.

The chosen models comprise a wide range of possible plume structures (Fig. 1). They include depth-dependent thermal expansivity and diffusivity, where expansivity decreases from top to bottom by a factor of eight and diffusivity increases by a factor of four following van Keken (2001). The viscosity increases by a factor of 30 below the 670-km phase transition. The temperature increase in the plume is 375 K and we assume that this causes a 200 times reduction in viscosity. The Rayleigh number (based on the background viscosity of the lower mantle and surface values of diffusivity and expansivity) is 1.52×10^6. The initial condition is based on a thermal boundary layer with 130 km initial thickness and a small perturbation at the plume axis. This thermal perturbation ΔT is applied for colatitude $\theta < \pi/8$ and has the form $\Delta T = 0.5\cos(8\theta)$.

Under these conditions, the plume rises through the lower mantle in approximately 30 Myr. The plume flow through the 670-km boundary is somewhat episodic even without the effects of phase transitions, but it reaches a nearly steady-state structure after approximately 80 Myr. In an early phase (P0h), the head is transiting and thinning in the upper-mantle. In a later quasi-steady-state phase (P0s), the plume has narrow upper and lower mantle tails and its head has spread laterally in the uppermost mantle.

Plumes P2s and P4s are quasi-steady-state stages of plumes where penetration into the upper mantle is partially (P2s) or completely (P4s) impeded. P2s and P4s have the same parameters as P0h and P0s, except for included phase boundaries at 410 and 670 km depth. For the 410-km boundary, we assume an exothermic phase boundary with constant Clapeyron slope of $+3$ MPa K^{-1}. For the 670-km boundary, we use an endothermic phase boundary with Clapeyron slopes of -2 MPa K^{-1} and -4 MPa K^{-1} for P2s and P4s, respectively. Plume P2s penetrates into the upper mantle but a portion of the original plume head remains in the uppermost lower mantle surrounding the plume conduit. For P4s, the phase boundary is sufficiently strong to force the plume to remain in the lower mantle, without an attendant surface expression.

Although the model dynamics assume strictly thermal plumes, we investigate the effects of entrainment of compositionally and seismically distinct material (Cobden *et al.* 2009) from the lowermost mantle in model $P0s^M$ and $P0s^P$. We assume that the anomalous components are confined to the plume cores, where temperatures are at least half of the maximum value at the plume axis. Two dense end-members are tested. The core of model $P0s^M$ has a basaltic composition representative of recycled oceanic crust (Perrillat *et al.* 2006). Model $P0s^P$ has a core with an iron and silica-rich primitive mantle composition (Anderson 1989). These dense chemical components will enhance the time-dependence of plume dynamics, including repeated head-like pulses and variable tail widths (Farnetani & Samuel 2005; Lin & van Keken 2006).

To map the thermal perturbations into seismic velocity anomalies, we calculate phase equilibria, density and elastic parameters as a function of temperature, pressure and composition using the thermodynamic method of Connolly (2005). We assume an isochemical pyrolitic composition (Sun 1982) and make a correction for the effects of anelasticity using a model with an Arrhenius temperature–pressure dependence (Cammarano *et al.* 2003; Goes *et al.* 2004). The procedure and uncertainties have been described in detail by Cobden *et al.* (2008, 2009). The mineral parameters and equation of state are from the 'sfo05' compilation for the CFMAS system (Stixrude & Lithgow-Bertelloni 2005; Khan *et al.* 2008).

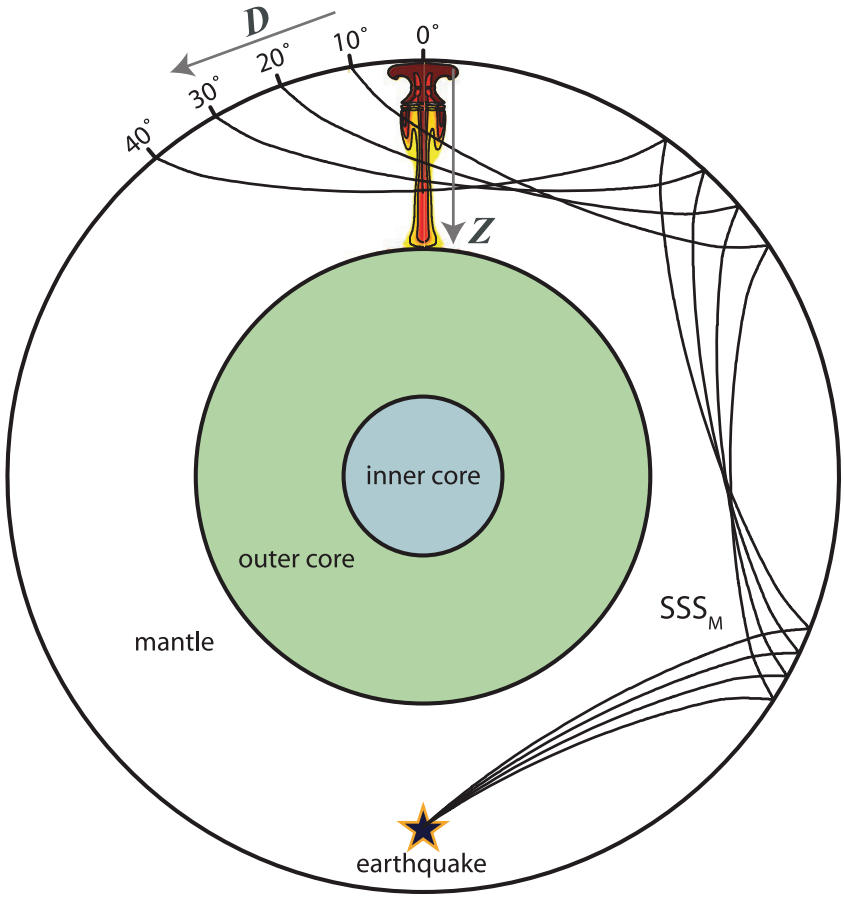

Figure 2. Plume P0h is shown as shear velocity perturbations with respect to PREM. The earthquake (star) is at 1000 km depth and located at the antipode of the plume. The regions shaded green and blue are the outer core and the inner core, respectively. The black lines are four geometric ray paths of SSS_M for epicentral distances of 190°, 200°, 210° and 220°, which correspond to angular distances D from the plume axis of 10°, 20°, 30° and 40°, respectively. The ray geometric crossing depths Z at the plume axis for these distances are 1077 km, 1563 km, 1857 km and 1989 km, respectively.

We limit our seismological modelling to this set of models. Plumes in nature are likely more complicated. They may not be axisymmetric due to plate motions (Steinberger 2000), can be thicker due to the formation of a thermal or compositional halo (Sleep 2006), the mapping of the thermal signal into seismic velocity may depend on the geotherm in the plume and in the surrounding mantle (Bunge 2005), and plumes may be either more time-dependent or more stationary. An extensive discussion on these variations is provided in Ito & van Keken (2007) but the current set is sufficiently realistic and diverse to test our hypothesis that wavefront healing may make robust lower mantle imaging of mantle plumes impossible.

3 WAVEFORM SIMULATIONS

We use the SHaxi method (Jahnke *et al.* 2008) to simulate the full 3-D shear wave (SH) motions in an axisymmetric shear velocity model. The waveform computation is performed on a 2-D grid of shear velocity variation and virtually expanded to 3-D spherical geometry by rotating the grid around the radial axis passing through the plume axis and the earthquake hypocentre (Fig. 2). The shear velocity anomalies associated with the plumes are assumed to be anomalies relative to the velocity structure in PREM.

Since the earthquake is at the antipode, we analyse the major-arc SSS phase (denoted as SSS_M) at angular distances D from the plume axis between 0° and 40° (i.e. epicentral distances between 180° and 220°). These waves have similar slownesses and cross the plume axis at the same depths Z as direct S waves at epicentral distances between 60° and 75°. By placing the earthquake at a depth of 1000 km, we minimize interference with other teleseismic phases. To determine the effects of plumes on shear waves, we compare the 3-D waveforms with the waveforms for PREM. The delay time of SSS_M, due to the presence of a plume in the mantle, is defined by the cross-correlation of plume and PREM synthetics.

Fig. 3 compares a selection of SHaxi seismograms for angular distances D between 1.5° and 9.5° computed for PREM and a model that includes the shear velocity perturbations of P0h. In this case (and for all other plumes), it is evident that SSS_M is delayed with respect to PREM when it propagates through the plume. This delay decreases with increasing D. When D is less than 3°, delay times are larger than 5 s but they diminish rapidly to 0.2 s when D is approximately 10°.

4 RESULTS AND CONCLUSIONS

Fig. 4 illustrates that the SSS_M traveltime delays depend on the morphology and shear velocity structure of the plumes. All plumes, except P4s, have heads in the upper mantle that are wider than 1000 km. For those models with upper mantle plume heads, SSS_M propagates through the head when $D < 5°$ and is delayed by

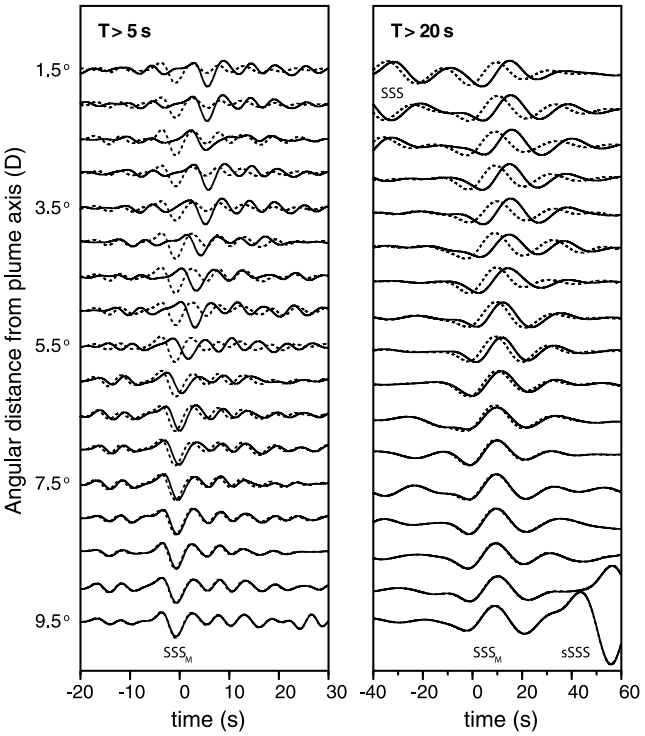

Figure 3. Waveforms (left-hand side) for periods longer than 5 s and (right-hand side) for periods longer than 20 s of SSS_M (aligned at time 0) between distances $D = 1.5^\circ$ and 9.5° for models PREM (dashed line) and model P0h (solid line). The labels SSS and sSSS indicate the arrival of the minor-arc SSS and its surface reflection within the time window around SSS_M at the shortest and longest distances.

6–12 s. Plumes P0s, $P0s^M$ and $P0s^P$ have similar shapes but the strength of their velocity anomalies differ near the plume axes and within the plume heads (compare Figs 1b, e, and f). The differences in internal velocity structures of plumes result in delay differences of several seconds when $D < 5^\circ$ (compare Figs 4b, e, and f). As soon as SSS_M propagates only through the plume tail, its delay decreases with increasing D and increasing Z. Plume P4s has a head below the 670-km phase transition. When SSS_M does not propagate through this head for D larger than 10°, its delay diminishes also. Thus, for all plumes, we find that SSS_M delay times are smaller than 0.2 s at distances larger than 10° when SSS_M traverses the plume tail at a depth larger than about 1000 km.

Just after traversing the plume tail in the lower mantle, SSS_M may be delayed by about 4 s. After the deceleration of the wavefront during its propagation through the plume, the indentation of the wavefront disappears due to diffraction. Consequently, the wave traveltime delay decreases exponentially with increasing propagation length L between the SSS_M crossing point on the plume axis and the seismic station on the surface. L is about 1500 km when D is 10°, or, equivalently, when SSS_M crosses the plume axis at a depth Z of about 1000 km. A propagation distance L of 1500 km is sufficiently long for complete wavefront healing and, thus, for shear wave delay times of 4 s just behind the lower mantle plume axis to diminish to immeasurably small values at the surface.

Delay times of teleseismic body-waves are the primary data for (tomographic) mapping of wave speed heterogeneity in the mantle. The signals of most seismic phases have emergent onsets or onsets hidden in the waveform coda of previously recorded phases. Hence, it is common practice to measure the delay times by waveform correlation akin to the procedure used in this paper. Typical measurement uncertainties exceed 0.5 s due to noise, waveform variability, uncertainties in earthquake location and origin time, and the poorly constrained effects of anisotropy and the heterogeneous crust on waveforms. Therefore, maximum delay times of 0.2 s due to plume tails in the lower mantle cannot be detected. While the broad (degree 2) low shear velocity provinces at the core–mantle boundary are robust structures, we demonstrate that wavefront healing reduces the effect of narrow plumes on traveltime delays of teleseismic waves to below seismic detection. This suggest that it is difficult to design experiments by which lower mantle plumes can be detected by seismological methods.

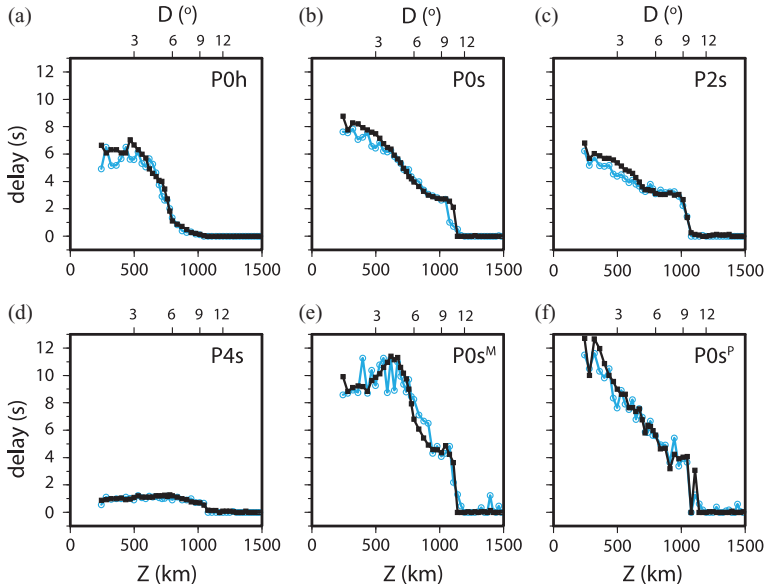

Figure 4. Traveltime delays as a function of the angular distance D from the plume axis (upper x-axis) and as a function of plume tail crossing depth Z (lower x-axis) for plumes (a) P0h, (b) P0s, (c) P2s, (d) P4s, (e) $P0s^M$ and (f) $P0s^P$. The traveltime delays measured at periods longer than 5 s and longer than 20 s are indicated by black squares and blue circles, respectively.

ACKNOWLEDGMENTS

We thank Michael Thorne for providing us with the code SHaxi for wave simulation and James O'Connolly for making the code PerPleX for velocity conversions available. We thank Norm Sleep and an anonymous reviewer for their constructive remarks. This research has been funded by NSF grant EAR-0855487 and a STFC postgraduate studentship (ES).

REFERENCES

Anderson, D.L., 1989. *Theory of the Earth,* Blackwell Scientific, Boston, MA.

Bunge, H.P., 2005. Low plume excess temperature and high core heat flux inferred from non-adiabatic geotherms in internally heated mantle circulation models, *Phys. Earth planet. Inter.,* **153**(1-3), 3–10.

Cammarano, F., Goes, S., Vacher, P. & Giardini, D., 2003. Inferring upper-mantle temperatures from seismic velocities, *Phys. Earth planet. Inter.,* **138,** 197–222.

Cobden, L., Goes, S., Cammarano, F. & Connolly, J.A.D., 2008. Thermochemical interpretation of one-dimensional seismic reference models for the upper mantle: evidence for bias due to heterogeneity, *Geophys. J. Int.,* **175,** 627–648.

Cobden, L., Goes, S., Ravenna, M., Styles, E., Cammarano, F., Gallagher, K. & Connolly, J.A.D., 2009. Thermochemical interpretation of 1-D seismic data for the lower mantle: the significance of nonadiabatic thermal gradients and compositional heterogeneity, *J. geophys. Res.,* **114**(B11309), doi:10.1029/2008JB006262.

Connolly, J.A.D., 2005. Computation of phase equilibria by linear programming: a tool for geodynamic modeling and its application to subduction zone decarbonation, *Earth planet. Sci. Lett.,* **236,** 524–541.

Dziewonski, A.M., Lekic, V. & Romanowicz, B., 2010. Mantle anchor structure: an argument for bottom up tectonics, *Earth planet. Sci. Lett.,* **299,** 69–79.

Farley, K.A. & Neroda, E., 1998. Noble gases in the Earth's mantle, *Annu. Rev. Earth Planet. Sci.,* **26,** 189–218.

Farnetani, C.G. & Samuel, H., 2003. Lagrangian structures and stirring in the Earth's mantle, *Earth planet. Sci. Lett.,* **206,** 335–348.

Farnetani, C.G. & Samuel, H., 2005. Beyond the thermal plume paradigm, *Geophys. Res. Lett.,* **32,** L07311, doi:10.1029/2005GL022360.

Foulger, G.R., Natland, J.H. & Anderson, D.L., 2005. A source for Icelandic magmas in remelted Iapetus crust, *J. Volc. Geotherm. Res.,* **141**(1-2), 23–44.

Goes, S., Cammarano, F. & Hansen, U., 2004. Synthetic seismic signature of thermal mantle plumes, *Earth planet. Sci. Lett.,* **218,** 403–419.

Hawkesworth, C.J., Kelley, S., Turner, S., Roex, A.L. & Storey, B., 1999. Mantle processes during Gondwana break-up and dispersal, *J. Afr. Earth Sci.,* **28,** 239–261.

Helmberger, D.V., Wen, L. & Ding, X., 1998. Seismic evidence that the source of the Iceland hotspot lies at the core-mantle boundary, *Nature,* **396,** 251–255.

Ito, G. & van Keken, P.E., 2007. Hotspots and melting anomalies, in *Treatise on Geophysics,* Vol. 7, pp. 371–436, Elsevier, Amsterdam.

Jahnke, G., Thorne, M.S., Cochard, A. & Igel, H., 2008. Global *SH*-wave propagation using a parallel axisymmetric spherical finite-difference scheme: application to whole mantle scattering, *Geophys. J. Int.,* **173,** 815–826.

Ji, Y. & Nataf, H.-C., 1998. Detection of mantle plumes in the lower mantle by diffraction tomography: Hawaii, *Earth planet. Sci. Lett.,* **159,** 99–115.

van Keken, P.E., 1997. Evolution of starting mantle plumes: a comparison between numerical and laboratory models, *Earth planet. Sci. Lett.,* **148,** 1–11.

van Keken, P.E., 2001. Cylindrical scaling for dynamical cooling models of the Earth, *Phys. Earth planet. Inter.,* **124,** 119–130.

van Keken, P.E. & Gable, C.W., 1995. The interaction of a plume with a rheological boundary: a comparison between two- and three-dimensional models, *J. geophys. Res.,* **100,** 20 291–20 302.

Khan, A., Connolly, J.A.D. & Taylor, S.R., 2008. Inversion of seismic and geodetic data for the major element chemistry and temperature of the Earth's mantle, *J. geophys. Res.,* **113,** B09308, doi:10.1029/2007JB005239.

King, S.D. & Ritsema, J., 2000. African hot spot volcanism: small-scale convection in the upper mantle beneath cratons, *Science,* **290,** 1137–1140.

King, S.D., Lee, C., van Keken, P.E., Leng, W., Zhong, S., Tan, E., Tosi, N., & Kameyama, M.C., 2010. A community benchmark for 2-D Cartesian compressible convection in the Earth's mantle, *Geophys. J. Int.,* **180,** 73–87.

Leng, W. & Zhong, S., 2010. Surface subsidence caused by mantle plumes and volcanic loading in large igneous provinces, *Earth planet. Sci. Lett.,* **291,** 207–214.

Lin, S.C. & van Keken, P.E., 2006. Dynamics of thermochemical plumes: 1. Plume formation and entrainment of a dense layer, *Geochem. Geophys. Geosyst.,* **7,** Q02006, doi:10.1029/2005GC001071.

Malcolm, A.E. & Trampert, J., 2011. Tomographic errors from wave front healing: more than just a fast bias, *Geophys. J. Int.,* **185**(1), 385–402.

Montelli, R., Nolet, G., Dahlen, F., Masters, G., Engdahl, E.R. & Hung, S.-H., 2004. Finite-frequency tomography reveals a variety of plumes in the mantle, *Science,* **303,** 338–343.

Nataf, H.-C. & VanDecar, J., 1993. Seismological detection of a mantle plume?, *Nature,* **364,** 115–120.

Perrillat, J.P., Ricolleau, A., Daniel, I., Fiquet, G., Mezouar, M., Guignot, N. & Cardon, H., 2006. Phase transformations of subducted basaltic crust in the upmost lower mantle, *Phys. Earth planet. Inter.,* **157**(1-2), 139–149.

Ribe, N., Davaille, A. & Christensen, U.R., 2007. Fluid dynamics of mantle plumes, in *Mantle Plumes,* pp. 1–48, Springer, Berlin.

Richards, M.A., Duncan, R.A. & Courtillot, V., 1989. Flood basalt and hotspot tracks: plume heads and tails, *Science,* **246,** 103–107.

Ritsema, J. & Allen, R.M., 2003. The elusive mantle plume, *Earth planet. Sci. Lett.,* **207,** 1–12.

Shen, Y., Solomon, S.C., Bjarnason, I.T. & Wolfe, C.J., 1998. Seismic evidence for a lower-mantle origin of the Iceland Plume, *Nature,* **395,** 62–65.

Sleep, N.H., 2006. Mantle plumes from top to bottom, *Earth-Sci. Rev.,* **77**(4), 231–271.

Steinberger, B., 2000. Plumes in a convecting mantle: models and observations for individual hotspots, *J. geophys. Res.,* **105**(B5), 11127–11152.

Steinberger, B. & O'Connell, R.J., 1998. Advection of plumes in mantle flow: implications for hot spot motion, mantle viscosity and plume distribution, *Geophys. J. Int.,* **132,** 412–434.

Stixrude, L. & Lithgow-Bertelloni, C., 2005. Thermodynamics of mantle minerals I. Physical properties, *Geophys. J. Int.,* **162,** 610–632.

Sun, S.-S., 1982. Chemical composition and origin of the Earth's primitive mantle, *Geochim. Cosmochim. Acta,* **46,** 179–192.

Wielandt, E., 1987. On the validity of the ray approximation for interpreting delay times, in *Seismic Tomography,* pp. 85–98, ed. Nolet, G., Reidel Publication Co., Dordrecht.

Wolfe, C.J., Bjarnason, I.T., VanDecar, J.C. & Solomon, S.C., 1997. Seismic structure of the Iceland mantle plume, *Nature,* **385,** 245–247.

Wolfe, C.J., Solomon, S.C., Laske, G., Collins, J.A., Detrick, R.S., Orcutt, J.A., Bercovici, D. & Hauri, E.H., 2009. Mantle shear-wave velocity structure beneath the Hawaiian Hot Spot, *Science,* **326,** 1388–1390.